JACS
JOURNAL OF THE AMERICAN CHEMICAL SOCIETY

ARTICLE

pubs.acs.org/JACS

Mechanistic Studies of O_2 Reduction Effected by Group 9 Bimetallic Hydride Complexes

Thomas S. Teets and Daniel G. Nocera*

Department of Chemistry, 6-335, Massachusetts Institute of Technology, 77 Massachusetts Avenue, Cambridge, Massachusetts 02139-4307, United States

Supporting Information

ABSTRACT: Synthetic and kinetic studies are used to uncover mechanistic details of the reduction of O_2 to water mediated by dirhodium complexes. The mixed-valence $Rh_2^{0,II}(tfepma)_2(CN^tBu)_2Cl_2$ (**1**, tfepma = $MeN[P(OCH_2CF_3)_2]_2$, CN^tBu = *tert*-butyl isocyanide) complex is protonated by HCl to produce $Rh_2^{II,II}(tfepma)_2(CN^tBu)_2Cl_3H$ (**2**), which promotes the reduction of O_2 to water with concomitant formation of $Rh_2^{II,II}(tfepma)_2(CN^tBu)_2Cl_4$ (**3**). Reactions of the analogous diiridium complexes permit the identification of plausible reaction intermediates. $Ir_2^{0,II}(tfepma)_2(CN^tBu)_2Cl_2$ (**4**) can be protonated to form the isolable complex $Ir_2^{II,II}(tfepma)_2(CN^tBu)_2Cl_3H$ (**5**), which reacts with O_2 to form $Ir_2^{II,II}(tfepma)_2(CN^tBu)_2Cl_3(OOH)$ (**6**). In addition, **4** reacts with O_2 to form $Ir_2^{II,II}(tfepma)_2(CN^tBu)_2Cl_2(\eta^2\text{-}O_2)$ (**7**), which can be protonated by HCl to furnish **6**. Complexes **6** and **7** were both isolated in pure form and structurally and spectroscopically characterized. Kinetics examination of hydride complex **5** with O_2 and HCl furnishes a rate law that is consistent with an HCl-elimination mechanism, where O_2 binds an Ir^0 center to furnish an intermediate η^2-peroxide intermediate. Dirhodium congener **2** obeys a rate law that not only is also consistent with an analogous HCl-elimination mechanism but also includes terms indicative of direct O_2 insertion and a unimolecular isomerization prior to oxygenation. The combined synthetic and mechanistic studies bespeak to the importance of peroxide and hydroperoxide intermediates in the reduction of O_2 to water by dirhodium hydride complexes.

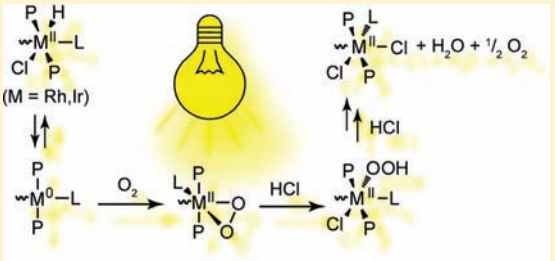

INTRODUCTION

Oxidase enzymes direct a complex series of four-proton, four-electron events in the reduction of molecular oxygen to water.[1] This same energy conversion chemistry is crucial to synthetic catalysts that recover the stored energy from water splitting[2−5] again with much complexity to be considered.[6] The mechanistic richness of the multiproton, multielectron reaction, coupled with its relevance to energy conversion, has led our group[7−11] and others[12−17] to explore molecular catalysts in a homogeneous solution because characterization of the catalytic species, the ability to tune catalytic properties, and the mechanism of action are in principle more easily investigated. The palette of molecular O_2-reduction chemistries reveals that the reduction of oxygen to water is favored in complexes that (i) are able to bind O_2, (ii) react in multielectron steps, and (iii) can couple this multielectron chemistry to proton transfer. For these reasons, hangman porphyrins with an appended acid or base functionality are especially effective O_2 reduction catalysts because they promote the requisite coupling of multielectron chemistry to proton transfer.[9,10,18,19]

A complementary strategy for multielectron, multiproton chemistry is to exploit bimetallic cooperativity using late transition metal bimetallic complexes,[20−22] and especially complexes that feature a stable two-electron mixed valence state. Until very recently, the multielectron chemistry of this broad class of bimetallic complexes has been focused on photocatalytic H_2 production,[23−25] halogen photoelimination,[26−30] and organometallic transformations.[31,32] However, in the course of studying dirhodium hydrido-chloride complexes in the context of HX splitting, we uncovered a strategy for the reduction of O_2 to water.[33] As outlined in Scheme 1, two-electron mixed valence complex $Rh_2^{0,II}(tfepma)_2(CN^tBu)_2Cl_2$ (**1**) reacts reversibly in its ground state with HCl to furnish $Rh_2^{II,II}(tfepma)_2(CN^tBu)_2Cl_3H$ (**2**); the reaction is facilitated by the coordinative unsaturation at the Rh^0 center in **1**. Once formed, hydrido-chloride complex **2** reacts with O_2 in the presence of additional HCl, producing $Rh_2^{II,II}(tfepma)_2(CN^tBu)_2Cl_4$ (**3**) and 1 equiv of H_2O. A photocycle can be realized by irradiating the product in THF, which regenerates **1**. The results demonstrate that two-electron mixed valency may promote the activation of oxygenated substrates.

A rhodium-bound hydroperoxide is a plausible intermediate in the conversion of O_2 to water by **2**, and Fukuzumi and coworkers have shown via kinetic studies that peroxo complexes are competent intermediates for oxygen reduction promoted by iridium complexes.[34] In our previous report on O_2 reduction mediated by dirhodium complex **2**, such intermediate species are not spectroscopically observed during the course of the reaction.

Received: July 24, 2011
Published: September 20, 2011

Scheme 1

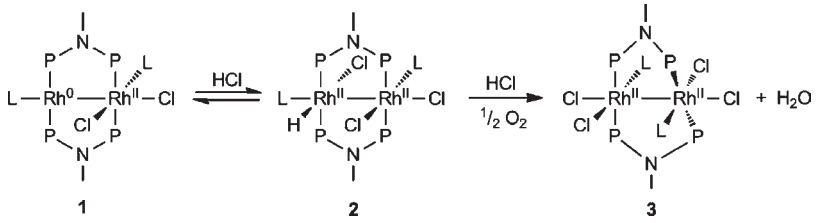

The insertion of O_2 into metal hydride bonds prevails for late transition metals,[35−43] especially in the context of aerobic oxidation catalysis.[44−46] Mechanistic studies and computations reveal three common mechanistic pathways for the insertion of O_2: (i) radical chain autoxidation,[38,44] (ii) HX dissociation followed by O_2 binding,[47] and (iii) direct H-atom abstraction by O_2.[45,48−50] In one case it was found that pathways (ii) and (iii) operate in parallel.[51]

We now employ model diiridium compounds to deduce mechanistic details of the reduction of O_2 by dirhodium hydride complex **2**. The third row analog of **2**, $Ir_2^{II,II}(tfepma)_2(CN^tBu)_2Cl_3H$ (**5**),[52] reacts cleanly with O_2 to form hydroperoxide complex $Ir_2^{II,II}(tfepma)_2(CN^tBu)_2Cl_3(OOH)$ (**6**), which is isolable and is amenable to structural and spectroscopic characterization. A side-on peroxide complex is obtained if the hydride is not present; $Ir_2^{II,II}(tfepma)_2(CN^tBu)_2Cl_2(\eta^2\text{-}O_2)$ (**7**) is formed from the reaction of O_2 with $Ir_2^{0,II}(tfepma)_2(CN^tBu)_2Cl_2$ (**4**). Additionally, the kinetic profile for the O_2 reduction reaction mediated by rhodium hydride complex **2** is consistent with the intermediacy of peroxide and hydroperoxide complexes akin to iridium models **6** and **7**. The results described here provide a mechanistic framework for O_2 reduction by bimetallic group 9 hydride complexes, and they show that O_2 insertion into metal hydride bonds can be a key step in the reduction of O_2 to water.

EXPERIMENTAL SECTION

General Considerations. All reactions involving air-sensitive materials were executed in a nitrogen-filled glovebox or on a high-vacuum manifold using solvents previously dried by passage through an alumina column under argon. The complexes $Rh_2^{0,II}(tfepma)_2(CN^tBu)_2Cl_2$ (**1**), $Ir_2^{0,II}(tfepma)_2(CN^tBu)_2Cl_2$ (**4**), and $Ir_2^{II,II}(tfepma)_2(CN^tBu)_2HCl_3$ (**5**) were prepared as described previously.[33,52] HCl (4 M in dioxane), 1,4-cyclohexadiene, and 2,2′-azobis(2-methylpropionitrile) (AIBN) were obtained from Sigma-Aldrich, whereas O_2 was purchased from Airgas and used as received. Elemental analyses were performed by Midwest Microlab LLC.

Physical Methods. NMR spectra were recorded at the MIT Department of Chemistry Instrumentation Facility on a Varian Mercury 300 NMR Spectrometer or a Varian Inova-500 NMR Spectrometer. $^{31}P\{^1H\}$ NMR spectra were referenced to an external standard of 85% D_3PO_4, and ^1H spectra were referenced to the residual proteo solvent resonances. UV−vis spectra were recorded at 293 K in THF solutions in quartz cuvettes on a Varian Cary 5000 UV−vis−NIR spectrophotometer. Extinction coefficients were determined over a concentration range of $\sim 10^{-6}-10^{-4}$ M, for which all compounds obeyed Beer's Law. IR spectra were recorded on a PerkinElmer Spectrum 400 FT-IR/FT-FIR Spectrometer outfitted with a Pike Technologies GladiATR attenuated total reflectance accessory with a monolithic diamond crystal stage and pressure clamp. Samples were suspended in Nujol for all IR measurements.

Kinetic Measurements. All kinetic experiments were monitored by UV−vis spectroscopy. Samples of appropriate concentrations were prepared in a nitrogen-filled glovebox and housed in quartz cuvettes sealed with a septum cap and containing a Teflon-coated magnetic stir bar. HCl solutions were introduced to the cuvette by syringe, and measured amounts of O_2 were injected using a gastight syringe. Samples were manually shaken to ensure complete mixing and equilibration of O_2. The cuvette was placed in a temperature-controlled cuvette holder with a magnetic stirrer, and reactions were monitored at 293 K by collecting single wavelength absorption data every 15 or 30 s, depending on the rate of the reaction. Data fitting and analysis were performed with the aid of the software OriginPro 8.

Preparation of $Ir_2^{II,II}(tfepma)_2(CN^tBu)_2Cl_3(OOH)$ (6). A J. Young NMR tube was charged with a solution of $Ir_2^{II,II}(tfepma)_2(CN^tBu)_2HCl_3$ (**5**) (42 mg, 0.026 mmol) in 0.7 mL of THF. The solution was freeze−pump−thaw degassed three times and then backfilled with ca. 1.5 atm of O_2. The reaction was monitored by $^{31}P\{^1H\}$ NMR, and after 2 h complete conversion was noted. The tube was freeze−pump−thaw degassed once to remove headspace O_2, and in the glovebox the contents were transferred to a 20-mL scintillation vial. The solvent was removed to afford a yellow solid, which was washed with 2 mL of hexane and dried in vacuo. Yield: 36 mg (84%). ^1H NMR (500 MHz, CD_3CN) δ/ppm: 7.32 (s, 1H), 5.34 (m, 2H), 4.99 − 5.15 (m, 4H) 4.94 (m, 4H), 4.77 (m, 2H), 4.68 (m, 2H), 4.62 (m, 2H), 2.93 (pseudoquintet, 6H), 1.45 (s, 9H), 1.41 (s, 9H). $^{31}P\{^1H\}$ NMR (202.5 MHz, CD_3CN) δ/ppm: 78.4−79.5 (m, 2P), 75.9−77.0 (m, 2P) (AA′BB′, 20 lines resolved, δ_{avg} = 77.7 ppm). UV−vis (THF): λ/nm ($\varepsilon/M^{-1}\,cm^{-1}$) 277 (26 000), 364 (3800), 402 (sh) (1200). IR (Nujol): $\tilde{\nu}_{C\equiv N}$ = 2185 cm^{-1}, $\tilde{\nu}_{O-H}$ = 3355 cm^{-1}. Anal. Calcd for $C_{28}H_{41}Cl_3F_{24}N_4O_{10}P_4Ir_2$: C, 20.21; H, 2.48; N, 3.37. Found: C, 20.41; H, 2.49; N, 3.25.

Preparation of $Ir_2^{II,II}(tfepma)_2(CN^tBu)_2Cl_2(\eta^2\text{-}O_2)$ (7). $Ir_2^{0,II}(tfepma)_2(CN^tBu)_2Cl_2$ (**4**) (50 mg, 0.031 mmol) was dissolved in 0.7 mL of THF and transferred to a J. Young NMR tube. The sample was degassed by three freeze−pump−thaw cycles and backfilled with ca. 1.5 atm of O_2. Upon mixing the tube manually, the color rapidly faded to a dull yellow-orange. The excess O_2 was removed by two freeze−pump−thaw cycles, and in the glovebox the contents of the NMR tube were transferred to a 20-mL scintillation vial. The solvent was removed in vacuo to afford a yellow-orange solid, which was redissolved in 2 mL of Et_2O/2 mL of hexane. Concentration in vacuo afforded a dark yellow solid, which was washed with 2 × 2 mL of hexane and dried in vacuo. Yield: 34 mg (67%). ^1H NMR (500 MHz, CD_3CN) δ/ppm: 5.05 − 5.14 (m, 4H), 4.95 (m, 4H) 4.52 − 4.78 (m, 8H), 2.85 (pseudoquintet, 6H), 1.46 (s, 9H), 1.43 (s, 9H). $^{31}P\{^1H\}$ NMR (121.5 MHz, CD_3CN) δ/ppm: 82.1 (m, 4P) (AA′BB′, 16 lines resolved, δ_{avg} = 82.1 ppm). UV−vis (THF): λ/nm ($\varepsilon/M^{-1}\,cm^{-1}$) 294 (12 000), 338 (sh) (7700), 397 (sh) (1600). IR (Nujol): $\tilde{\nu}_{C\equiv N}$ = 2148, 2174 cm^{-1}. Anal. Calcd for $C_{28}H_{40}Cl_2F_{24}N_4O_{10}P_4Ir_2$: C, 20.66; H, 2.48; N, 3.44. Found: C, 20.83; H, 2.37; N, 3.29.

X-ray Crystallographic Details. Single crystals of **6** were obtained by synthesizing the complex in CD_3CN and allowing the sample to stand at room temperature, and crystals of **7** were obtained in an

dx.doi.org/10.1021/ja2069196 |J. Am. Chem. Soc. 2011, 133, 17796–17806

Table 1. Crystallographic Summary for Complexes 6 and 7

	6	7
Formula	$C_{28}H_{41}Cl_3F_{24}Ir_2N_4O_{10}P_4$	$C_{28}H_{40}Cl_2F_{24}Ir_2N_4O_{10}P_4$
fw, g/mol	1664.28	1627.82
Temperature	100(2) K	100(2) K
cryst. syst.	Monoclinic	Monoclinic
space group	$P2_1/n$	$P2_1$
color	yellow	yellow
a (Å)	13.003(2)	12.4449(13)
b (Å)	10.798(2)	18.0315(19)
c (Å)	18.699(4)	12.9712(13)
α (deg)	90	90
β (deg)	91.086(3)	117.313(2)
γ (deg)	90	90
V (Å^3)	2625.0(8)	2586.2(5)
Z	2	2
no. refl.	50603	57482
no. unique refl.	4479	15121
R_{int}	0.0911	0.0566
$R1$[a] (all data)	0.0645	0.0434
$wR2$[b] (all data)	0.1216	0.0797
$R1$ [$(I > 2\sigma)$]	0.0493	0.0353
$wR2$ [$(I > 2\sigma)$]	0.1175	0.0760
GOF[c]	1.079	0.995
Flack param.	—	−0.0100(42)

[a] $R1 = \Sigma||F_o| - |F_c||/\Sigma|F_o|$. [b] $wR2 = (\Sigma(w(F_o^2 - F_c^2)^2)/\Sigma(w(F_o^2)^2))^{1/2}$. [c] GOF = $(\Sigma\, w(F_o^2 - F_c^2)^2/(n-p))^{1/2}$ where n is the number of data and p is the number of parameters refined.

analogous fashion from Et_2O. The crystals were mounted on a Bruker three circle goniometer platform equipped with an APEX detector. A graphite monochromator was employed for wavelength selection of the Mo Kα radiation (λ = 0.710 73 Å). The data were processed and refined using the program SAINT supplied by Siemens Industrial Automation. Structures were solved by Patterson methods in SHELXS and refined by standard difference Fourier techniques in the SHELXTL program suite (6.10 v., Sheldrick G. M., and Siemens Industrial Automation, 2000). Hydrogen atoms bonded to carbon were placed in calculated positions using the standard riding model and refined isotropically; all non-hydrogen atoms were refined anisotropically. In the structure of **6**, the O−H proton was tentatively located in the difference map, restrained to a distance of 0.84 Å from the oxygen nucleus and refined isotropically. In the structure of **6**, the $(OOH)^-$ ligand and equatorial Cl^- ligand were disordered about a crystallographically imposed inversion center, and three of the four crystallographically independent $-OCH_2CF_3$ groups were modeled as two-part disorders. The (1,2) and (1,3) distances of all disordered parts were restrained to be similar using the SADI command; the rigid-bond restraints SIMU and DELU were also used on disordered parts. Unit cell parameters, morphology, and solution statistics for the structures of **6** and **7** are summarized in Table 1. All thermal ellipsoid plots are drawn with carbon-bound hydrogen atoms omitted for clarity.

RESULTS

Reaction of 2 with O_2 and HCl. The reaction of $Rh_2^{II,II}(tfepma)_2(CN^tBu)_2Cl_3H$ (**2**) with O_2 and HCl[33] is briefly summarized here and is shown pictorially in Scheme 1. Complex **2** is formed reversibly by treatment of $Rh_2^{0,II}(tfepma)_2(CN^tBu)_2Cl_2$ (**1**) with HCl and is indefinitely stable to HCl. The equilibrium

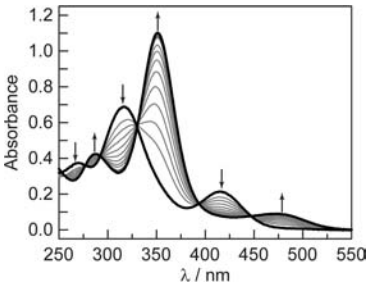

Figure 1. Spectral evolution during the reaction of **2** (40 μM) with O_2 (0.80 atm) in the presence of HCl (55 mM). The reaction was carried out in THF at 293 K, and spectra were recorded every 5 min.

Chart 1

4 + NEt_3•HCl ⇄ **5** + NEt_3	$K_{eq} = 5 \times 10^{-4}$	(i)
NEt_3 + HCl ⇄ NEt_3•HCl	$K_{eq} = 8.3 \times 10^{9}$	(ii)
4 + HCl ⇄ **5**	$K_{eq} = 4 \times 10^{6}$	(iii)

constant for the addition of HCl to complex **1** is determined to be 1.8×10^2 by ^{1}H NMR integration. Upon introduction of O_2 gradual conversion to $Rh_2^{II,II}(tfepma)_2(CN^tBu)_2Cl_4$ (**3**) is observed; $^{31}P\{^1H\}$ and ^{1}H NMR show that **3** is formed in >90% yield. Furthermore, 1 equiv of D_2O is exclusively formed as the deuterium-containing product from DCl solutions, confirming that **2** effects the reduction of O_2 to water along the way to forming **3**. Photolysis of **3** when isolated from excess HCl and O_2 drives the regeneration of **1** to complete a photocycle.

The reaction of **2** with O_2 and HCl can be monitored by UV−vis absorption spectroscopy. The electronic spectra of authentic samples of **2** and **3** are depicted in Figure S1 for reference. The spectrum of **2** consists of three distinct maxima at 270, 317, and 414 nm. Figure 1 shows the spectral evolution when complex **2**, in the presence of 55 mM HCl, is treated with 0.80 atm of O_2 at 293 K. Over the time course of the 70-min reaction, features attributed to $Rh_2^{II,II}$ complex **3** grow in, with isosbestic points maintained at 256, 276, 292, 330, 394, and 447 nm, in good agreement with the predicted isosbestic values from the authentic spectra shown in Figure S1. The final spectrum, which is a good match for that of an authentic sample of **3**, indicates near-quantitative conversion to **3**. These observations suggest clean conversion of **2** to **3** at micromolar concentrations, and the presence of the isosbestic points indicates that substantial concentrations of intermediate species do not accrue during the course of the reaction.

HCl Addition to $Ir_2^{0,II}$ Complex 4. Treatment of $Ir_2^{0,II}(tfepma)_2(CN^tBu)_2Cl_2$ (**4**) with HCl forms the isolable iridium analog to **2**, $Ir_2^{II,II}(tfepma)_2(CN^tBu)_2Cl_3H$ (**5**), as previously documented.[52] The equilibrium constant for HCl addition to **4** to form **5** was measured using the thermodynamic cycle shown in Chart 1, analogous to a method used by Bercaw and DuBois to determine protonation equilibria for monometallic rhodium hydride complexes.[53] The equilibrium constant was measured in acetonitrile, owing to the sufficient solubility of amine hydrochloride salts and the ready availability of the relevant acid dissociation constants in this solvent. The equilibrium constant for (i) in Chart 1 was determined by ^{1}H NMR integration after treating $Ir_2^{0,II}$ complex **4** with NEt_3•HCl in CD_3CN. The equilibrium

Scheme 2

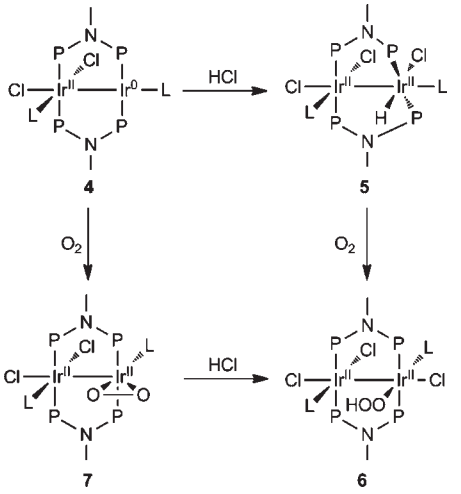

constant of (ii) is calculated from known pK_a values of HCl[54] and triethylammonium[55] in acetonitrile. Reaction (iii) in Chart 1 is simply the sum of (i) and (ii), such that the HCl-addition equilibrium constant is the product of the K_{eq}'s for (i) and (ii). In this manner, a K_{eq} of 4×10^6 is obtained for the addition of HCl to diiridium complex **4** to furnish **5**.

Reaction of 5 with O_2 To Form $Ir_2^{II,II}(tfepma)_2(CN^tBu)_2Cl_3$-(OOH) (6). Scheme 2 summarizes the oxygen reactivity of the diiridium complexes that will be considered here. Complex **5** (with no additional HCl) reacts cleanly with O_2 to form $Ir_2^{II,II}$-$(tfepma)_2(CN^tBu)_2Cl_3(OOH)$ (**6**), which can be isolated in 84% yield and is determined to be pure by multinuclear NMR and elemental analysis. The $^{31}P\{^1H\}$ NMR spectrum of **6**, depicted in Figure S4, shows two closely spaced multiplets best described as arising from an AA′BB′ spin system; this type of splitting has been observed in other asymmetric $Ir_2^{II,II}$ complexes.[52] The ^1H NMR spectrum shows the expected resonances from ligand protons, with two distinct *tert*-butyl resonances indicating chemical inequivalency of the two *tert*-butyl isocyanide ligands. In addition, a singlet at 7.32 ppm is attributed to the OO−*H* proton. The IR spectrum shows a single resolvable $\tilde{\nu}_{C\equiv N}$ stretch at 2185 cm^{-1} and a weak, broad $\tilde{\nu}_{O-H}$ stretch at 3355 cm^{-1}.

Hydroperoxide complex **6** has been crystallographically characterized, and its structure is shown in Figure 2. The structure of **6** contains a crystallographically imposed inversion center, such that half of the molecule is present in the asymmetric unit and the hydroperoxide ligand is disordered with the equatorial chloride ligand. The resulting structure shows two octahedral Ir^{II} centers, where the octahedra are eclipsed and the Ir(1)−Ir(1A) distance is 2.7492(8) Å. The O(5)−O(6) distance is 1.509(19) Å, similar to but slightly longer than in the case of other structurally characterized transition metal terminal hydroperoxide complexes.[44,45,56−63] The poor O−O bond length precision results from the aforementioned disorder, but nonetheless this distance is consistent with an oxygen−oxygen single bond. The structure of **6** represents, to the best of our knowledge,[64] the first example of a structurally characterized iridium hydroperoxide complex.

The reaction of iridium hydride complex **5** with O_2 to form hydroperoxide **6** is also conveniently monitored by UV−vis absorption spectroscopy. The overlaid spectra of **5** and **6** are depicted in Figure S2, showing that the absorption maxima are similar [λ_{max} = 285 nm (**5**), 277 nm (**6**)], though for the

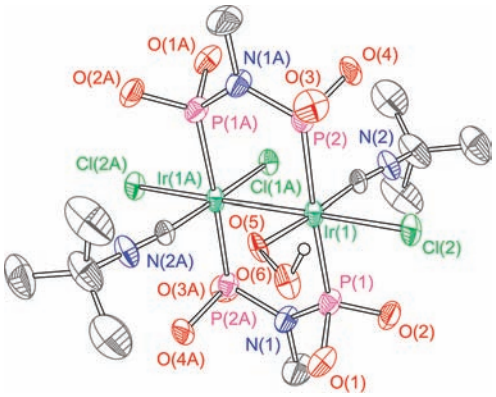

Figure 2. Thermal ellipsoid plot for **6**. Ellipsoids are shown at the 50% probability level with $-CH_2CF_3$ groups and carbon-bound hydrogen atoms omitted for clarity. Data were collected at 100 ± 2 K.

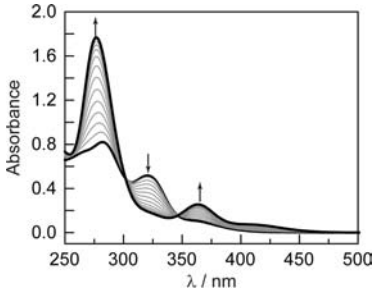

Figure 3. Spectral evolution during the reaction of **5** (67 μM) with O_2 (0.40 atm). The reaction was carried out in THF at 293 K, and spectra were recorded every 5 min.

wavelength of maximum absorbance the molar absorptivity in hydroperoxide complex **6** is much greater [ε = 12 000 M^{-1} cm^{-1} (**5**), 26 000 M^{-1} cm^{-1} (**6**)]. After introduction of 0.40 atm of O_2 to a 67 μM solution of **5**, the absorption spectra evolve as shown in Figure 3. Over time, the features of **6** appear; the final spectrum (t = 65 min) is a good match to the authentic spectrum of **6** (Figure S2). Isosbestic points maintained at 301 and 347 nm are in good agreement with their expected positions, and once again their presence shows that intermediate species persist at very low concentrations during the course of the reaction or that no intermediates are involved in the conversion.

Reaction of 4 with O_2 To Form $Ir_2^{II,II}(tfepma)_2(CN^tBu)_2Cl_2$-($\eta^2$-$O_2$) (7). As shown in Scheme 2, $Ir_2^{0,II}$ complex **4** reacts directly with O_2 to form a side-on peroxo complex, $Ir_2^{II,II}$-$(tfepma)_2(CN^tBu)_2Cl_2(\eta^2\text{-}O_2)$ (**7**). The reaction is quite rapid, and within minutes $^{31}P\{^1H\}$ NMR of the crude reaction mixture reveals complete conversion. Analytically pure **7** is isolated in 67% yield and can withstand several hours of in vacuo drying without O_2 loss. The $^{31}P\{^1H\}$ NMR spectrum (Figure S5) shows two closely spaced multiplets suggestive of an AA′BB′ spin system, where in this case the ν_A and ν_B values are nearly coincident. The ^1H NMR spectrum shows the expected resonances arising from tfepma and CN^tBu ligands, with only minimal shifting relative to $Ir_2^{0,II}$ precursor **4**. The IR spectrum shows two closely spaced $\tilde{\nu}_{C\equiv N}$ stretching frequencies at 2148 and 2174 cm^{-1}, though the $\tilde{\nu}_{O-O}$ stretch, expected to occur in the range of 800−900 cm^{-1}, is obscured by strong features from the supporting ligands. The electronic absorption spectrum in

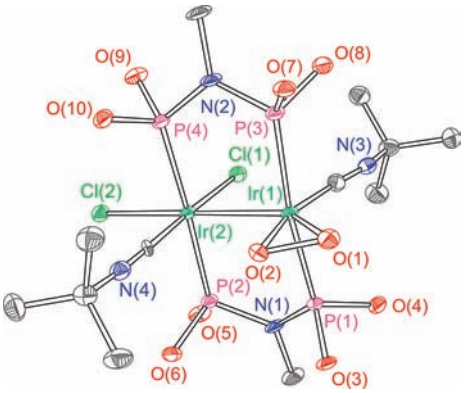

Figure 4. Thermal ellipsoid plot for **7**. Ellipsoids are shown at the 50% probability level with $-CH_2CF_3$ groups and hydrogen atoms omitted for clarity. Data were collected at 100 ± 2 K.

Figure S3 reveals three closely spaced bands characteristic of d^7-d^7 $Ir_2^{II,II}$ complexes.

X-ray crystallography confirms the structure of **7**, as shown in Figure 4. Complex **7** represents the first structurally characterized example of O_2 binding by a two-electron mixed valence diiridium complex. The η^2-O_2 binding mode is reminiscent of the uptake of dioxygen by Vaska's complex[65−67] and other related Ir^I complexes,[68−72] as opposed to the μ-O_2 diiridium-peroxide cyclic motif that results when an $Ir^I\cdots Ir^I$ complex is treated with O_2.[73,74] The O(1)−O(2) internuclear distance of 1.480(5) Å is consistent with these previous examples and is demonstrative of a fully reduced O_2^{2-} ligand. It should be noted that librational disorder can lead to inaccuracies in crystallographically determined O−O bond distances in η^2-O_2 complexes; in particular the observation of abnormally short O−O bonds is a recurring problem.[75] However, the reported O−O bond distance in **7** is not noticeably short for a peroxide moiety, and the low temperature of the data collection (100 K) should minimize these effects. The O(1)−O(2)−Ir(1) and O(2)−O(1)−Ir(1) bond angles of 70.6(2)° and 67.6(2) °, respectively, necessitate a severe distortion from octahedral geometry at the Ir(1) center. The Ir(1)−Ir(2) distance is 2.7498(4) Å, nearly identical to that of **6** and falling in line with other $Ir_2^{II,II}$ complexes characterized recently.

Peroxide complex **7** is reactive toward HCl, forming hydroperoxide **6** as the major product as judged by the $^{31}P\{^1H\}$ NMR spectrum of the reaction mixture. Several side products are also observed, though they can be attributed to HCl-induced decomposition of hydroperoxide complex **6**, as determined from an independent reaction of **6** with HCl. This reactivity establishes the bottom reaction pathway shown in Scheme 2 and gives the possibility that peroxide complex **7** forms as an intermediate during the direct oxygenation of hydride complex **5** to hydroperoxide **6**.

Rate Law for the Reaction of $Rh_2^{II,II}HCl_3$ (2) with HCl and O_2 To Form $Rh_2^{II,II}Cl_4$ (3). The kinetic profile for the reaction of dirhodium hydride complex **2** with HCl and O_2 was determined. Based on previous NMR experiments,[33] complex **2** exists as a mixture of two isomers in a ca. 7:1 ratio. The equilibrium between the two isomers is established within minutes, indicating that interconversion is rapid relative to the time scale of reaction with O_2 and thus it has no bearing on the observed kinetics for O_2 reduction. The reaction proceeds as described in Scheme 1, and it is conveniently monitored by tracking the production of **3** as indicated by the growth of the absorbance at 350 nm. Figure 5 shows a representative kinetic trace for the reaction of **2** with O_2 and HCl, in this case with 1.6 atm of O_2 and 5.5 mM of HCl. As expected, the absorbance at 350 nm grows in over time, and with these pseudo-first-order conditions a monoexponential time course is observed. With these conditions, k_{obs} = 0.12 min^{-1}.

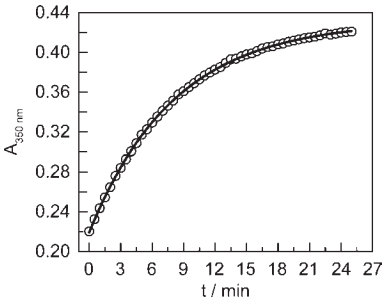

Figure 5. Representative kinetic trace for the reaction of **2** with O_2 (1.6 atm) and HCl (5.5 mM), showing the change in the absorbance at 350 nm ($A_{350\ nm}$) vs time. The solid line shows the best-fit monoexponential curve.

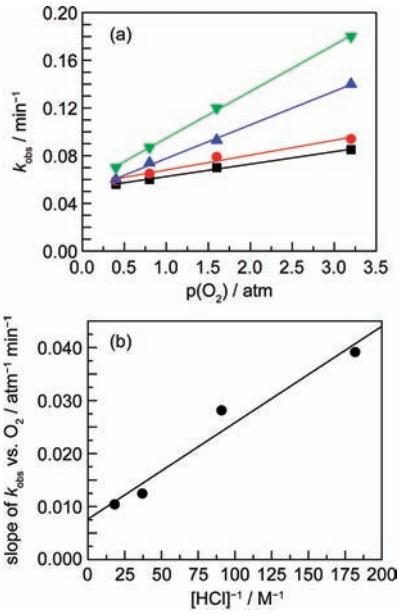

Figure 6. (a) Dependence of k_{obs} on p(O_2) for the reaction of **2** with O_2 and HCl, with the [HCl] at 5.5 mM (green ▼), 11 mM (blue ▲), 27 mM (red ●) and 55 mM (black ■). The solid lines show the best-fit lines for each data set. (b) The slopes of the best-fit lines of k_{obs} vs p(O_2) from (a) are plotted against $[HCl]^{-1}$. The best-fit line is shown.

Figure 6a shows the dependence of k_{obs} on the partial pressure of O_2, p(O_2), at four different HCl concentrations. The values for k_{obs} depend on both O_2 partial pressure and HCl concentration. At a constant [HCl], the value of k_{obs} varies linearly with p(O_2), though in all cases a nonzero *y*-intercept is observed. By inspection of Figure 6a, it is clear that the *y*-intercept of the four plots is invariant to the [HCl], and best-fit lines yield *y*-intercepts ranging between 0.050 and 0.055 min^{-1}, with no systematic trend. As shown in Figure 6b, the slopes of the plots in Figure 6a vary linearly with $[HCl]^{-1}$, with a nonzero intercept of 0.008(2) atm^{-1} min^{-1}. This shows that there are two first-order O_2 terms in the rate law, one which is inverse first-order in HCl, the other

dx.doi.org/10.1021/ja2069196 |*J. Am. Chem. Soc.* 2011, 133, 17796–17806

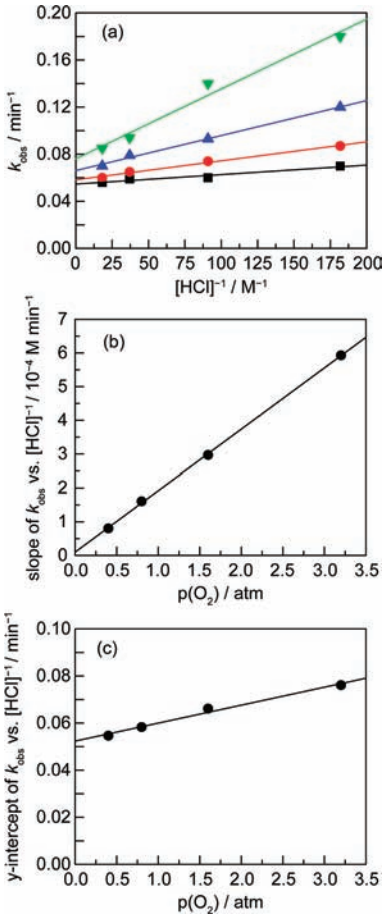

Figure 7. (a) Dependence of k_{obs} on $[HCl]^{-1}$ for the reaction of **2** with O_2 and HCl, with $p(O_2)$ at 0.4 atm (black ■), 0.8 atm (red ●), 1.6 atm (blue ▲), and 3.2 atm (green ▼). Data are the same as those depicted in Figure 6. The solid red lines show the best-fit lines for each data set. (b) The slopes of the best-fit lines of k_{obs} vs $[HCl]^{-1}$ from (a) are plotted against $p(O_2)$. The best-fit line is shown. (b) The *y*-intercepts of the best-fit lines of k_{obs} vs $[HCl]^{-1}$ from (a) are plotted against $p(O_2)$. The best-fit line is shown.

zero-order. Further insight is provided by plotting k_{obs} vs $[HCl]^{-1}$, as shown in Figure 7a. Qualitative visual inspection of Figure 7a reveals that both the slopes and intercepts of the depicted plots vary with $p(O_2)$. Figure 7b shows the dependence of the slopes on $p(O_2)$, and a strict first-order trend is observed, dictating that there is a single inverse first-order HCl term in the rate law which is also first-order in O_2. In Figure 7c, the *y*-intercepts from Figure 7a are plotted vs $p(O_2)$. A linear dependence with a nonzero *y*-intercept is seen, suggesting two HCl-independent terms in the rate law.

Taken together, the data in Figures 6 and 7 give rise to a three-term rate law, whose form is given by

$$\text{Rate} = k_1[\mathbf{2}][O_2][HCl]^{-1} + k_1'[\mathbf{2}][O_2] + k_1''[\mathbf{2}] \qquad (1)$$

The best-fit lines in Figures 6 and 7 provide estimates for the three rate constants. The first rate constant, k_1, is determined from the slope of either Figure 6b or 7b and is found to be $1.8(3) \times 10^{-4}$ M atm^{-1} min^{-1}. The rate constant k_1' is readily determined from the slope of Figure 7c, with a value of 0.0076(6) atm^{-1} min^{-1}. And finally, the *y*-intercept of Figure 7c gives the zero-order rate constant k_1'', which has a value of 0.052(1) min^{-1},

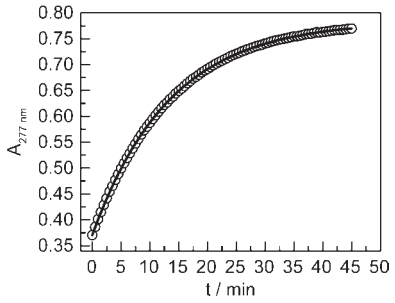

Figure 8. Representative kinetic trace for the reaction of **5** with O_2 (3.2 atm) showing the change in the absorbance at 277 nm ($A_{277\ nm}$) vs time. The solid line shows the best-fit monoexponential curve.

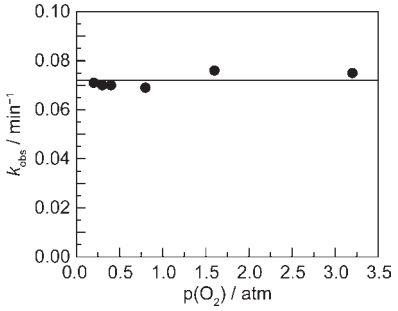

Figure 9. Dependence of k_{obs} on $p(O_2)$ for the reaction of **5** with O_2. The horizontal line is drawn at the average of value of $k_{obs} = 0.072$ min^{-1}.

matching the average value of the *y*-intercepts from the individual plots in Figure 6a.

In addition to the dependencies described above, the reaction of **2** with O_2 and HCl was conducted in the presence of the radical inhibitor BHT (1 mM), which was found to have a minimal effect on the observed kinetics. In the absence of BHT, the reaction of **2** with 3.2 atm of O_2 and 55 mM of HCl gives a k_{obs} of 0.085 min^{-1}, whereas in the presence of 1 mM of BHT the observed pseudo-first-order rate constant was 0.077 min^{-1}. Furthermore, it should be noted that the kinetic traces do not show any deviations at later time points attributed to the formation of the product water. Thus, at least at the concentrations that are formed during the conversion of **2** to **3**, the evolved H_2O has no effect on the observed kinetics.

Rate Law for the Reaction of $Ir_2^{II,II}HCl_3$ (5) with O_2 To form $Ir_2^{II,II}Cl_3(OOH)$ (6). The reaction rate of $Ir_2^{II,II}(tfepma)_2(CN^tBu)_2Cl_3H$ (**5**) with O_2 was monitored as a function of O_2 partial pressure. Figure 8 shows a representative trace for the conversion of **5** to **6** with 3.2 atm of O_2 and in the absence of HCl. The reaction is monitored at 277 nm, where **6** absorbs strongly. The data in Figure 8 can be satisfactorily fit to a monoexponential function, as shown by the best-fit monoexponential curve. Figure 9 shows that the observed rate constant, k_{obs}, has a zero-order dependence on O_2 concentration. The average value is 0.072 min^{-1} with no systematic variation in the range of 0.20 to 3.2 atm of O_2. Thus, for the reaction of **5** with O_2 to form **6**, a simple rate law is obtained,

$$\text{Rate} = k_2[\mathbf{5}] \qquad (2)$$

The reaction of **5** with O_2 is strongly inhibited by added HCl, as determined from initial reaction rates with varying HCl concentrations. Figure 10 shows the dependence of k_{obs} (determined from initial rates) as a function of inverse HCl concentration.

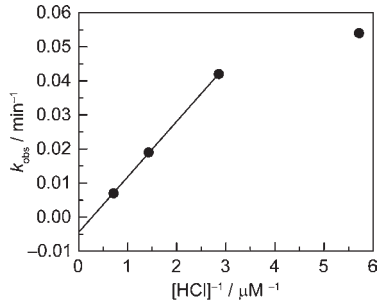

Figure 10. Plot of k_{obs} vs $[HCl]^{-1}$ for the reaction of **5** with O_2 (0.80 atm). Rate constants were calculated from initial rate data. A best-fit line to the three highest [HCl] values is shown.

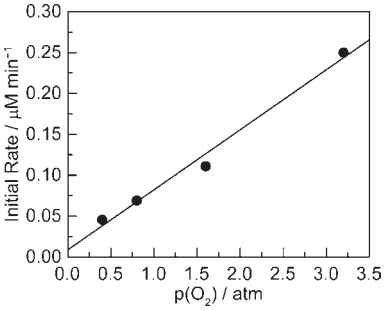

Figure 11. Plot of initial rate vs $p(O_2)$ for the reaction of **5** with O_2 in the presence of HCl (1.4 μM). The $[\mathbf{5}]_o$ is 9.7 μM.

The data are clearly linear at the upper range of HCl concentrations, indicative of a concentration regime where the reaction is inverse first-order in HCl. With added HCl, the reaction becomes first-order in O_2, as indicated by the initial rate data in Figure 11. A linear dependence is observed, and the *y*-intercept is very nearly zero, suggesting a single term in the rate law. The above indicate that, in the presence of HCl, the conversion of **5** to **6** exhibits the following rate law,

$$\text{Rate} = k_3[\mathbf{5}][O_2][HCl]^{-1} \quad (3)$$

The value of k_3, determined from Figure 11, is 2.0×10^{-8} M atm^{-1} min^{-1}.

Radical inhibitors have minimal effect on the observed rate constants. Addition of 1 mM of BHT gave a k_{obs} of 0.070 min^{-1}, and with 1 mM of 1,4-cyclohexadiene k_{obs} = 0.069 min^{-1}, with 0.80 atm of O_2. These values are nearly identical to the average value of 0.072 min^{-1} over the range of O_2 concentrations (Figure 9). The radical initiator AIBN has a slight inhibitory effect on the reaction: at 80 μM AIBN, k_{obs} = 0.064 min^{-1}, and at 1 mM AIBN, k_{obs} = 0.050 min^{-1}.

DISCUSSION

Reactivity of Diridium Complexes with O_2. With the goal of understanding the mechanism of O_2 reduction mediated by dirhodium hydride complex **2**, we first investigated oxygenation reactions with diiridium complexes. $Ir_2^{0,II}$ complex **4** and its corresponding protonation product **5** are structurally analogous to their dirhodium brethren **1** and **2**. In addition, diiridium hydride complex **5**, unlike its dirhodium relative **2**, is thermally stable in the absence of HCl and as such is readily isolated. This feature allowed for an isolated study of the reactivity of **5** with O_2, without interference of subsequent HCl reactivity.

Addition of O_2 to **5** gives hydroperoxide complex **6**, which itself can be isolated. Recognizing the possibility of binding of O_2 by the M^0 center, the reactions of O_2 with $M_2^{0,II}$ complexes **1** and **4** were investigated. The reaction of dirhodium complex **1** with O_2 under ambient conditions fails to produce a stable O_2 adduct, and a gradual and nonspecific decomposition is observed. However, diiridium complex **4** reacts rapidly and cleanly with O_2, forming the isolable η^2-peroxide complex **7**. Taken together, complexes **6** and **7** represent plausible structural models for intermediate species involved in the reduction of O_2 mediated by dirhodium complex **2**. As we show below they are indeed kinetically reasonable intermediates for the reaction sequence.

Mechanism of Formation of Iridium Hydroperoxide 6. We begin with a discussion of the reaction of the diridium hydride complex **5** with O_2 to form hydroperoxide complex **6**. The mechanistic considerations for this reaction will serve as a framework for interpreting the results of the dirhodium system. Radical-based mechanisms, which have been invoked previously in select examples of O_2-insertion chemistry,[38,44,76] can be excluded. The reaction of **5** with O_2 is unaffected by the radical inhibitors BHT and 1,4-cyclohexadiene; the reaction is actually slightly inhibited by AIBN, which should accelerate a radical reaction.

The kinetic profile for the conversion of **5** to **6** takes on two different forms, depending on whether HCl is present as an additive. All of the observations described above are consistent with the HCl-elimination mechanism that is summarized by the following reaction sequence,

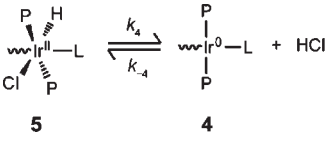

5 **4** (4)

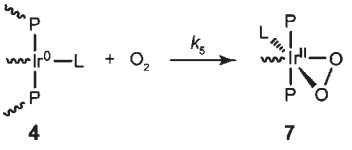

4 **7** (5)

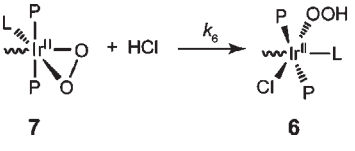

7 **6** (6)

Reversible HCl elimination from hydride complex **5** produces $Ir_2^{0,II}$ complex **4**, which binds O_2 via the reactive Ir^0 center to yield η^2-peroxide complex **7**. Our ability to isolate complex **7** and its apparent thermal stability, even under vacuum, suggest irreversible binding of O_2. Complex **7** is protonated by HCl to form the hydroperoxide complex **6**. The rate law for the three-step mechanism described by eqs 4–6 is

$$\frac{d[\mathbf{6}]}{dt} = \frac{k_4 k_5[\mathbf{5}][O_2]}{k_{-4}[HCl] + k_5[O_2]} \quad (7)$$

In the absence of HCl, the $k_{-4}[HCl]$ term in the denominator approaches zero, equivalent to the HCl elimination step (4)

Scheme 3

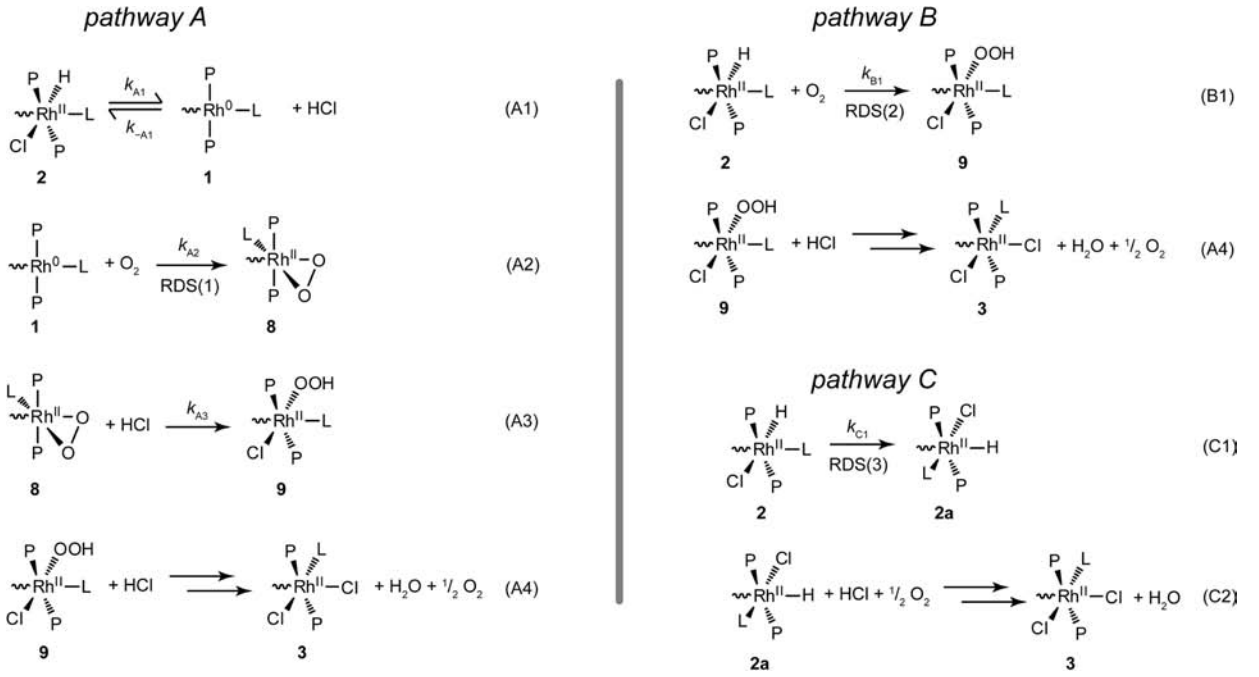

becoming irreversible and rate limiting. In this case, the rate law becomes

$$\frac{d[\mathbf{6}]}{dt} = \frac{k_4 k_5[\mathbf{5}][O_2]}{k_5[O_2]} = k_4[\mathbf{5}] \quad (8)$$

equivalent to the rate law shown in eq 2, with $k_2 = k_4$. When HCl is present, the k_{-4}[HCl] term becomes large relative to $k_5[O_2]$, and O_2-binding becomes the rate-determining step, leading to the following rate law,

$$\frac{d[\mathbf{6}]}{dt} = \frac{k_4 k_5[\mathbf{5}][O_2]}{k_{-4}[HCl]} \quad (9)$$

This simplified rate law is equivalent to that of eq 3, with $k_3 = k_4k_5/k_{-4}$. The data in Figures 10 and 11 predict a first-order dependence on O_2 and an inverse first-order dependence on HCl, when **5** is reacted with **6** in the presence of added HCl. Thus the rate behavior predicted from the mechanistic sequence of reactions of eqs 4 − 6 is realized experimentally, where the O_2 order depends on the presence or absence of added HCl, which itself exhibits an inverse-first order.

The reactivity that we have established here, and summarized in Scheme 2, lends credence to the proposed mechanism for the conversion of **5** to **6**. We predict the equilibrium constant $K_4 = k_4/k_{-4}$ to be quite small on the basis that (i) the formation of hydride complex **5** from $Ir_2^{0,II}$ complex **4** and HCl appears quantitative and (ii) complex **5** is readily isolated and found to be stable in the absence of HCl.[52] Indeed, the measured value for K_4, the inverse of the HCl-addition equilibrium constant (Chart 1), is 2.5×10^{-7}. Nonetheless, the kinetic studies suggested HCl reductive elimination prior to oxygenation. Motivated by these results, we have independently verified that $Ir_2^{0,II}$ complex **4**, formed by HCl elimination from **5**, reacts rapidly and quantitatively with O_2. The reaction forms the isolable complex $Ir_2^{II,II}(tfepma)_2(CN^tBu)_2Cl_2(\eta^2\text{-}O_2)$ (**7**), which can be treated with HCl to form hydroperoxide complex **6** as the major product. Thus, the intermediate species **4** and **7** have both been isolated, and their reactivity is consistent with the proposed mechanism that is constructed from kinetic rate profiles.

Mechanism of O_2 Reduction by Dirhodium Complex 2. The foregoing mechanistic studies on the diiridium analogs provide a framework for interpreting the dirhodium system, for which no intermediate species can be isolated. The kinetic studies described above revealed a complex three-term rate law, given in eq 1. The rate law indicates that three distinct reaction pathways operate in parallel for the conversion of **2** to **3** when reacted with O_2 and HCl. The three parallel reaction pathways shown in Scheme 3 fit well with the kinetic data and furnish the rate law

$$\frac{d[\mathbf{3}]}{dt} = \frac{k_{A1}k_{A2}[\mathbf{2}][O_2]}{k_{-A1}[HCl]} + k_{B1}[\mathbf{2}][O_2] + k_{C1}[\mathbf{2}] \quad (10)$$

Equation 10 is equivalent to eq 1, with $k_1 = k_{A1}k_{A2}/k_{-A1}$, $k_1' = k_{B1}$ and $k_1'' = k_{C1}$. We will first focus on the first term of the rate law, which is consistent with the reaction sequence pathway A of Scheme 3. This mechanism is analogous to that of the diiridium analogs (eqs 4 − 6). The inverse HCl dependence dictates an HCl elimination reaction prior to the rate-determining step, and the first-order O_2 term mandates that the reaction with O_2 is rate-limiting. These results are consistent with the formation of peroxide complex **8**. Subsequent elementary steps occur beyond the rate-determining step and as such have no kinetics impact, though the protonation of **8** (reaction A3, Scheme 3), would seem likely based on the reactivity characterized for the diiridium analogs. Another possibility, which cannot be discounted on the basis of the kinetics data, is that the proposed peroxide intermediate **8** continues on to produce water without being protonated to a hydroperoxide, as has been suggested by Fukuzumi and collaborators in work on iridium complexes.[34] However, such a scheme would require liberation of OH^- and formation of a high-valent rhodium oxo, leading us to still favor the route we have proposed in Scheme 3. The second term in the rate law is

dx.doi.org/10.1021/ja2069196 |J. Am. Chem. Soc. 2011, 133, 17796–17806

first-order in O_2 and requires an alternate reaction sequence to occur in parallel. Here again, the formation of hydroperoxide intermediate **9** is invoked, in this case via direct reaction of hydride complex **2** and O_2 (B1). Hydroperoxide formation via direct H-atom abstraction has been implied from kinetic studies on Pd^{II} complexes[45] and has been described computationally.[48,49] Other computational[50] and experimental[51] studies have also shown that the HCl reductive elimination and H-atom abstraction pathways are close in energy and can operate competitively, as observed here. The subsequent reactivity of **9** to result in the production of H_2O with concomitant formation of $Rh^{II,II}Cl_4$ complex **3** occurs after the rate-determining steps for these two pathways. Thus we cannot speak definitively about the precise nature of the reaction (A4). We speculate two possibilities: (i) evolution of a rhodium−hydroxide complex followed by protonolysis to release H_2O, or (ii) protonation of **9** to release H_2O_2, which is rapidly dismutated to O_2 and H_2O. Additional studies will be required to lend credence to either of these suggestions.

The third term of the rate law in eq 1, which dictates the mechanism for the other parallel reaction pathway that results in the conversion of **2** to **3**, is zero-order with respect to both O_2 and HCl. Accordingly there is little that can be said definitively about this parallel pathway, other than that the net conversion prior to the rate-determining step is a unimolecular reaction of **2**. We favor the sequence shown in pathway C of Scheme 3, involving rate-limiting isomerization to form hydride complex **2a**. We observed previously by NMR studies that solutions of **2** contain ~14% of a minor product, which rapidly equilibrates with the major species.[33] Since the interconversion of the two isomers is rapid, we cannot invoke this observed minor isomer as the reacting species in reaction (C1). However, there is the possibility that a third isomer, perhaps involving an axial hydride, is formed in minor equilibrium and is reactive toward O_2. Other possibilities for the rate-limiting unimolecular step involve dissociation of either a chloride or CN^tBu ligand to open up a coordination site at one of the rhodium centers and cannot be explicitly ruled out. Addition of $(NBu_4)Cl$ or CN^tBu to reaction mixtures causes deleterious side reactions of **2**, making it impossible to assess an inhibitory effect of either of these ligands on any of the parallel pathways in the reaction sequence. Reaction (C2), leading to the conversion of **2a** to **3**, is necessarily ill-defined since it occurs past the unimolecular rate-limiting step and as such does not give rise to an observed order in either HCl or O_2. Reaction (C2) may involve H-atom abstraction by O_2, which must be faster in pathway C than in pathway B. We have not crystallographically observed axial hydride ligands in any related complexes, though it is worth noting that, in the previously reported crystal structures of dirhodium complexes **1**−**3**, the axial Rh−Cl bond distances are consistently 0.08−0.12 Å longer than the adjacent equatorial Rh−Cl.[33] This observation confirms a sizable trans influence of the Rh−Rh bond, which would weaken the Rh−H bond in an axial isomer and could lead to a lower activation barrier for H-atom abstraction subsequent to formation of a minor axial hydride isomer. One final possibility, which also cannot be ruled out, is that an isomer of **2** also undergoes the HCl reductive elimination pathway, but with HCl-elimination as the rate-determining step. This pathway would be identical to pathway A, but would originate from a different isomer of **2** and would effectively involve irreversible, rate-determining HCl elimination, as opposed to pre-equilibrium HCl loss. This would give rise to a term in the rate law which is only first-order in complex **2**, with no O_2 or HCl dependence, and would require that the barrier for reductive elimination of the participating isomer be higher than that of **2**. Ultimately, computational studies will be focused toward distinguishing these various possibilities for the third rate law term of eq 1.

With these mechanistic proposals in hand, some quantitative differences between the dirhodium and diiridium O_2-activation chemistries become apparent. In particular, the protonation equilibrium constants and O_2-binding rate constants are distinct between the dirhodium and diiridium complexes. As described earlier, the equilibrium constant for HCl addition to $Rh_2^{0,II}$ complex **1** is 1.8×10^2, whereas for $Ir_2^{0,II}$ complex **4** the analogous K_{eq} is over 4 orders of magnitude higher at 4×10^6. The observed rate constants for the HCl-reductive elimination pathways (eqs 4 − 6 and Scheme 3A) are given by k_{O_2}/K_{eq}, where k_{O_2} is the rate constant for O_2 binding to the $M_2^{0,II}$ complex and K_{eq} is the equilibrium constant for HCl addition to the $M_2^{0,II}$ species. Provided that HCl is present in sufficient quantities such that HCl-elimination is reversible and not rate-determining, the values for the O_2-binding rate constants, k_5 and k_{A2}, can be extracted. For $Ir_2^{0,II}$ complex **4**, the O_2-binding rate constant $k_5 = 8 \times 10^{-2}$ atm^{-1} min^{-1}, whereas for $Rh_2^{0,II}$ complex **1** the analogous rate constant is quite similar at $k_{A2} = 3.2 \times 10^{-2}$ atm^{-1} min^{-1}. Thus the major kinetic difference between the HCl-reductive elimination pathways for the dirhodium and diiridium complexes is found in the equilibrium constants for HCl elimination, and not in the intrinsic difference in the rate constant for binding of O_2 to form the metal−peroxide intermediate.

In summary, the results described herein establish a mechanistic basis for understanding important steps in the four-electron, four-proton reduction of O_2 to water mediated by group 9 bimetallic hydride complexes. Considerable insight into the mechanism of O_2 reduction mediated by the dirhodium hydride complex $Rh_2^{II,II}(tfepma)_2(CN^tBu)_2Cl_3H$ is acquired by examining its diiridium congeners owing to the ability to isolate and characterize plausible reaction intermediates. The results of synthesis and kinetics, taken together, permit us to delineate pathways for the insertion of O_2 into the metal−hydride bonds. We have determined that O_2-binding by the M^0 center, to furnish an η^2-O_2 complex, is a key step in these transformations. The O_2 reactivity at the square-planar Rh^0 and Ir^0 centers is facilitated by the unsaturated coordination environment. In the case of the dirhodium system, kinetic studies reveal two additional competing pathways for O_2 insertion, one involving direct H-atom abstraction and the other proceeding through an isomeric species. Subsequent work will aim to unveil pathways by which the hydroperoxide intermediates selectively liberate H_2O as the reduced oxygen species.

■ ASSOCIATED CONTENT

Supporting Information. Electronic spectra for **2**, **3**, and **5**−**7**; $^{31}P\{^1H\}$ NMR spectra of **6** and **7**; and the crystallographic information files (CIF) for **6** and **7**. This material is available free of charge via the Internet at http://pubs.acs.org.

■ AUTHOR INFORMATION

Corresponding Author
nocera@mit.edu

■ ACKNOWLEDGMENT

This work was supported by NSF Grant CHE-1112154. Grants from the NSF also supported the MIT Department of

Chemistry Instrumentation Facility (CHE-9808061 and DBI-9729592). T.S.T. acknowledges the Fannie and John Hertz Foundation for a graduate research fellowship. Yogesh Surendranath is acknowledged for helpful discussions.

REFERENCES

(1) Kaila, V. R. I.; Verkhovsky, M. I.; Wikström, M. *Chem. Rev.* **2010**, *110*, 7062–7081.
(2) Cook, T. R.; Dogutan, D. K.; Reece, S. Y.; Surendranath, Y.; Teets, T. S.; Nocera, D. G. *Chem. Rev.* **2010**, *110*, 6474–6502.
(3) Nocera, D. G. *Inorg. Chem.* **2009**, *48*, 10001–10017.
(4) Lewis, N. S.; Nocera, D. G. *Proc. Natl. Acad. Sci. U.S.A.* **2006**, *103*, 15729–15735.
(5) Winter, M.; Brodd, R. J. *Chem. Rev.* **2004**, *104*, 4245–4270.
(6) Adler, S. B. *Chem. Rev.* **2004**, *104*, 4791–4843.
(7) Chang, C. J.; Deng, Y.; Shi, C.; Chang, C. K.; Anson, F. C.; Nocera, D. G. *Chem. Commun.* **2000**, 1355–1356.
(8) Chang, C. J.; Loh, Z.-H.; Shi, C.; Anson, F. C.; Nocera, D. G. *J. Am. Chem. Soc.* **2004**, *126*, 10013–10020.
(9) Rosenthal, J.; Nocera, D. G. *Acc. Chem. Res.* **2007**, *40*, 543–553.
(10) McGuire, R., Jr.; Dogutan, D. K.; Teets, T. S.; Suntivich, J.; Shao-Horn, Y.; Nocera, D. G. *Chem. Sci.* **2010**, *1*, 411–414.
(11) Dogutan, D. K.; Stoian, S. A.; McGuire, R., Jr.; Schwalbe, M.; Teets, T. S.; Nocera, D. G. *J. Am. Chem. Soc.* **2011**, *133*, 131–140.
(12) Chang, C. K.; Liu, H. Y.; Abdalmuhdi, I. *J. Am. Chem. Soc.* **1984**, *106*, 2725–2726.
(13) Collman, J. P.; Wagenknecht, P. S.; Hutchinson, J. E. *Angew. Chem., Int. Ed.* **1994**, *33*, 1537–1554.
(14) Anson, F. C.; Shi, C.; Steiger, B. *Acc. Chem. Res.* **1997**, *30*, 437–444.
(15) Fukuzumi, S.; Kotani, H.; Lucas, H. R.; Doi, K.; Suenobu, T; Peterson, R. L.; Karlin, K. D. *J. Am. Chem. Soc.* **2010**, *132*, 6874–6875.
(16) Soo, H. S.; Komor, A. C.; Iavarone, A. T.; Chang, C. J. *Inorg. Chem.* **2009**, *48*, 10024–10035.
(17) Halime, Z.; Kotani, H.; Li, Y.; Fukuzumi, S.; Karlin, K. D. *Proc. Natl. Acad. Sci. U.S.A.* **2011**, *108*, 13990–13994.
(18) Rosenthal, J.; Nocera, D. G. *Prog. Inorg. Chem.* **2007**, *55*, 483–544.
(19) Dogutan, D. K.; Bediako, D. K.; Teets, T. S.; Schwalbe, M.; Nocera, D. G. *Org. Lett.* **2010**, *12*, 1036–1039.
(20) Shibasaki, M.; Yamamoto, Y., Eds. *Multimetallic Catalysts in Organic Synthesis*; Wiley VCH: Weinheim, 2004.
(21) Broussard, M. E.; Juma, B.; Train, S. G.; Peng, W.-J.; Laneman, S. A.; Stanley, G. G. *Science* **1993**, *260*, 1784–1788.
(22) Gray, T. G.; Veige, A. S.; Nocera, D. G. *J. Am. Chem. Soc.* **2004**, *126*, 9760–9768.
(23) Heyduk, A. F.; Nocera, D. G. *Science* **2001**, *293*, 1639–1641.
(24) Esswein, A. J.; Veige, A. S.; Nocera, D. G. *J. Am. Chem. Soc.* **2005**, *127*, 16641–16651.
(25) Heyduk, A. F.; Nocera, D. G. *J. Am. Chem. Soc.* **2000**, *122*, 9415–9426.
(26) Heyduk, A. F.; Macintosh, A. M.; Nocera, D. G. *J. Am. Chem. Soc.* **1999**, *121*, 5023–5032.
(27) Cook, T. R.; Esswein, A. J.; Nocera, D. G. *J. Am. Chem. Soc.* **2007**, *129*, 10094–10095.
(28) Cook, T. R.; Surendranath, Y.; Nocera, D. G. *J. Am. Chem. Soc.* **2009**, *131*, 28–29.
(29) Teets, T. S.; Lutterman, D. A.; Nocera, D. G. *Inorg. Chem.* **2010**, *49*, 3035–3043.
(30) Teets, T. S.; Neumann, M. P.; Nocera, D. G. *Chem. Commun.* **2011**, *47*, 1485–1487.
(31) Esswein, A. J.; Veige, A. S.; Piccoli, P. M. B.; Schultz, A. J.; Nocera, D. G. *Organometallics* **2008**, *27*, 1073–1083.
(32) Veige, A. S.; Gray, T. G.; Nocera, D. G. *Inorg. Chem.* **2005**, *44*, 17–26.
(33) Teets, T. S.; Cook, T. R.; McCarthy, B. D.; Nocera, D. G. *J. Am. Chem. Soc.* **2011**, *133*, 8114–8117.
(34) Fukuzumi, S.; Kobayashi, T.; Suenobu, T. *J. Am. Chem. Soc.* **2010**, *132*, 118666–118667.
(35) Roberts, H. L.; Symes, W. R. *J. Chem. Soc. A* **1968**, 1450–1453.
(36) Johnston, L. E.; Page, J. A. *Can. J. Chem.* **1969**, *47*, 4241–4246.
(37) Gillard, R. D.; Heaton, B. T.; Vaughan, D. H. *J. Chem. Soc. A* **1970**, 3126–3130.
(38) Endicott, J. F.; Wong, C.-L.; Inoue, T.; Natarajan, P. *Inorg. Chem.* **1979**, *18*, 450–454.
(39) Atlay, M. T.; Preece, M.; Strukul, G.; James, B. R. *Chem. Commun.* **1982**, 406–407.
(40) Atlay, M. T.; Preece, M.; Strukul, G.; James, B. R. *Can. J. Chem.* **1983**, *61*, 1332–1338.
(41) Bakac, A. *J. Am. Chem. Soc.* **1997**, *119*, 10726–10731.
(42) Thyagarajan, S.; Incarvito, C. D.; Rheingold, A. L.; Theopold, K. H. *Chem. Commun.* **2001**, 2198–2199.
(43) Cui, W.; Wayland, B. B. *J. Am. Chem. Soc.* **2006**, *128*, 10350–10351.
(44) Wick, D. D.; Goldberg, K. I. *J. Am. Chem. Soc.* **1999**, *121*, 11900–11901.
(45) Denney, M. C.; Smythe, N. A.; Cetto, K. L.; Kemp, R. A.; Goldberg, K. I. *J. Am. Chem. Soc.* **2006**, *128*, 2508–2509.
(46) Konnick, M. M.; Gandhi, B. A.; Guzei, I. A.; Stahl, S. S. *Angew. Chem., Int. Ed.* **2006**, *45*, 2904–2907.
(47) Konnick, M. M.; Stahl, S. S. *J. Am. Chem. Soc.* **2008**, *130*, 5753–5762.
(48) Keith, J. M.; Nielson, R. J.; Oxgaard, J.; Goddard, W. A., III. *J. Am. Chem. Soc.* **2005**, *127*, 13172–13179.
(49) Keith, J. M.; Muller, R. P.; Kemp, R. A.; Goldberg, K. I.; Goddard, W. A., III; Oxgard, J. *Inorg. Chem.* **2006**, *45*, 9631–9633.
(50) Popp, B. V.; Stahl, S. S. *J. Am. Chem. Soc.* **2007**, *129*, 4410–4422.
(51) Konnick, M. M.; Decharin, N.; Popp, B. V.; Stahl, S. S. *Chem. Sci.* **2011**, *2*, 326–330.
(52) Teets, T. S.; Cook, T. R.; McCarthy, B. D.; Nocera, D. G. *Inorg. Chem.* **2011**, *50*, 5223–5233.
(53) Wilson, A. D.; Miller, A. J. M.; DuBois, D. L.; Labinger, J. A.; Bercaw, J. E. *Inorg. Chem.* **2010**, *49*, 3918–3926.
(54) Izutsu, K. *Electrochemistry in Nonaqueous Solutions*; Wiley-VCH: Weinheim, 2009; Chapter 3.
(55) Kaljurand, I.; Kütt, A.; Sooväli, L.; Rodima, T.; Mäemets, V.; Leito, I.; Koppel, I. A. *J. Org. Chem.* **2005**, *70*, 1019–1028.
(56) Carmona, D.; Lamata, M. P.; Ferrer, J.; Modrega, J.; Perales, M.; Lahoz, F. J.; Atencio, R.; Oro, L. A. *Chem. Commun.* **1994**, 575–576.
(57) Wada, A.; Harata, M.; Hasegawa, K.; Jitsuwaka, K.; Masuda, H.; Mukai, M.; Kitagawa, T.; Einaga, H. *Angew. Chem., Int. Ed.* **1998**, *37*, 798–799.
(58) Takahashi, Y.; Hashimoto, M.; Hikichi, S.; Akita, M.; Moro-oka, Y. *Angew. Chem., Int. Ed.* **1999**, *38*, 3074–3077.
(59) Akita, M.; Miyaji, T.; Hikichi, S.; Moro-oka, Y. *Chem. Lett.* **1999**, *28*, 813–814.
(60) Guzei, I. A.; Bakac, A. *Inorg. Chem.* **2001**, *40*, 2390–2393.
(61) Miyaji, T.; Kujime, M.; Hikichi, S.; Moro-oka, Y.; Akita, M. *Inorg. Chem.* **2002**, *41*, 5286–5295.
(62) Rostovsev, V. V.; Henling, L. M.; Labinger, J. A.; Bercaw, J. E. *Inorg. Chem.* **2002**, *41*, 3608–3619.
(63) Ahijado, M.; Braun, T.; Noveski, D.; Kocher, N.; Neumann, B.; Stalke, D.; Stammler, H.-G. *Angew. Chem., Int. Ed.* **2005**, *44*, 6947–6951.
(64) As determined from a search of the Cambridge Structural Database (WebCSD v1.1.1).
(65) Vaska, L. *Science* **1963**, *140*, 809–810.
(66) La Placa, S. J.; Ibers, J. A. *J. Am. Chem. Soc.* **1965**, *87*, 2581–2586.
(67) Lebel, H.; Jadjel, C.; Bélanger-Gariépy, F.; Schaper, F. *J. Organomet. Chem.* **2008**, *693*, 2645–2648.
(68) McGinnety, J. A.; Doedens, R. J.; Ibers, J. A. *Inorg. Chem.* **1967**, *12*, 2243–2250.
(69) Wang, H.-H.; Pignolet, L. H.; Reedy, P. E.; Olmstead, M. M.; Balch, A. L. *Inorg. Chem.* **1987**, *26*, 377–383.
(70) Barbaro, P.; Bianchini, C.; Laschi, F.; Midollini, S.; Moneti, S.; Scapacci, G.; Zanello, P. *Inorg. Chem.* **1994**, *33*, 1622–1630.

(71) Doux, M.; Ricard, L.; Le Floch, P.; Jean, Y. *Orgnanometallics* **2005**, *24*, 1608–1613.
(72) Crestani, M. G.; Steffen, A.; Kenwright, A. M.; Batsanov, A. S.; Howard, J. A. K.; Marder, T. B. *Organometallics* **2009**, *28*, 2904–2914.
(73) Vaartstra, B. A.; Xiao, J.; Cowie, M. *J. Am. Chem. Soc.* **1990**, *112*, 9425–9426.
(74) Xiao, J.; Santarsiero, B. D.; Vaartstra, B. A.; Cowie, M. *J. Am. Chem. Soc.* **1993**, *115*, 3212–3220.
(75) Cramer, C. J.; Tolman, W. B.; Theopold, K. H.; Rheingold, A. L. *Proc. Natl. Acad. Sci. U.S.A.* **2003**, *100*, 3635–3640.
(76) Boisvert, L.; Denney, M. C.; Hanson, S. K.; Goldberg, K. I. *J. Am. Chem. Soc.* **2009**, *131*, 15802–15814.